Use of Series Negative Impedance to Cancel the Effect of Equivalent Grid Impedance on the Grid-Connected Inverter Stability in the DPGS

Yuanbin He
Research Institute of Electrical Engineering and Automation
Hangzhou Dianzi University
Hangzhou, China
yuanbinhe@hdu.edu.cn

Chun-tak Lai, Shu-hung Chung
Centre for Smart Energy Conversion and Utilization Research
City University of Hong Kong
Kowloon, Hong Kong
eeshc@cityu.edu.hk

Xin Zhang
School of Electrical and Electronic Engineering
Nanyang Technological University
Singapore
xinzhangee@gmail.com

Weimin Wu
Research Institute of Electronic Automation
Shanghai Maritime University
Shanghai, China
wmwu@shmtu.edu.cn

***Abstract*—An active grid impedance cancellator is proposed to suppress the effect of the grid disturbance and stabilize the distributed power generation (DPG) grid-connected inverters operating under the weak grid. Harmonic interaction between the DPG inverter and the grid is thereby avoided owing to the cancellation of equivalent grid impedance. The impedance cancellator composed of a full-bridge dc-ac converter without passive filtering elements is connected in series at the inverter output to simulate a negative virtual grid impedance. In addition, an active damping function is integrated to suppress the filter resonance of the inverter. In the paper, the system configuration and the control strategy of the impedance cancellator are introduced. The power consumption of the cancellator is also evaluated. A single-phase grid-connected inverter prototype has been built to verify the effectiveness of the proposed method. The experimental results show a good agreement with the theoretical knowledge.**

Keywords—inverter; LCL filter; grid impedance cancellator; active damping

I. INTRODUCTION

Grid-connected inverters are generally voltage source converters with an output power filter. Among various types of filters, third-order inductive-capacitive-inductive (LCL) filter has become popular, as it requires smaller reactive elements than the classical inductive (L) and inductive-capacitive (LC) filters [1]-[2]. For these types of inverters, the ac output current regulation faces the challenge of the filter resonance. Thus, many prior arts, such as passive and active damping techniques, have been proposed to tackle the filter resonance. Among them, active damping techniques are preferable, as they do not cause extra power dissipation and can achieve resonance suppression flexibly. However, active damping performance strictly relies on the ratio between the filter resonance frequency and the sampling frequency in the digitally-controlled inverter [3]-[4]. Moreover, because the filter resonance frequency will vary as the equivalent grid impedance changes, it would give challenges to develop an effective active damping function that can ensure the operational stability of the inverter both in stiff- and weak-grid conditions. On the other hand, distributed-power-generation (DPG) inverters installed at the same point-of-common-coupling (PCC) are coupled with each other due to the grid impedance and would lead to harmonic interaction and current circulation between each other [5]-[10]. Multiple reactive elements in the inverter output filters, such as filtering capacitive and inductive components as shown in Fig. 1, could also exhibit multiple resonant frequencies due to the existence of the grid impedance. Thus, the system stability will be subject to multiple resonant behavior rather than the single resonance caused by the local filter.

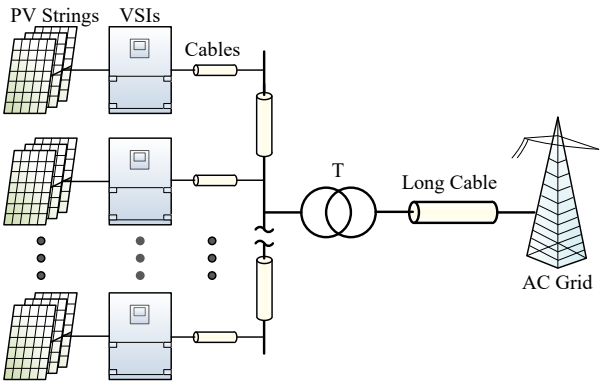

(a) System configuration.

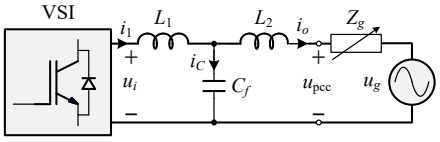

(b) Equivalent single inverter.

Fig. 1 Typical PV DPG system.

The paper presents an LCL filter-based grid-connected inverter with active cancellation of equivalent grid impedance based on the concept of series active filter. The cancellator consists of a bidirectional dc-ac converter and features: 1) no need to use additional passive LC filtering elements, 2)

The work described in this paper was supported by grants from the National Natural Science Foundation of China (NSFC) under Award 51707051, and from the Research Grants Council (RGC) of the Hong Kong Special Administrative Region, China under NSFC/RGC Joint Research Scheme (Project No.: N_CityU128/15), and (Project No.: 51561165013).

cancellation of the effect of grid impedance, 3) strong harmonic suppression against grid disturbance, and 4) active damping function to ease the burden of the inverter current control. The reshaped inverter with an LCL filter appears as a well-damped one without equivalent grid impedance. In Sec. II, the proposed system configuration is described, and the control strategy of the grid impedance cancellator is examined. An inverter prototype with the grid impedance cancellator is then built. Its dynamic behaviors under the weak grid are discussed in Sec. III. The conclusion follows in Sec. IV.

II. Operational Principle

A. System Configuration

The LCL filter-based current-controlled grid-connected inverter with proposed grid impedance cancellator for typical PV application is shown in Fig. 2. The grid impedance cancellator, implemented by a full bridge dc-ac converter with no need of extra passive filtering elements, is connected in series at the inverter output, which aims to counteract the effect of grid impedance and eliminate the harmonic voltage at the inverter output voltage, u_o.

Although four switching devices are used in the full bridge-based impedance cancellator, each switching device only needs to sustain a very low dc capacitor voltage, u_{dc}, such as 30~50 V, which is determined by the small harmonic voltage at the PCC, $u_{pcc,h}$, indirectly. Thus, the total power dissipation of the switching devices, S_1~S_4, is much lower than the main switching network of the inverter.

B. Control Strategy

Because the compensated ac voltage, u_{ic}, is the direct output voltage of the dc-ac converter as shown in Fig. 2, the unity gain-based harmonic voltage at the PCC is directly feedforwarded into the modulator so as to generate equivalent ac output voltage as presented in Fig. 3, where the notch filter with the center frequency ω_0 is used to eliminate the dominant line frequency component of the PCC voltage so as to sustain a very low harmonic output voltage, and T_S is the sampling cycle in synchronous with the switching operation.

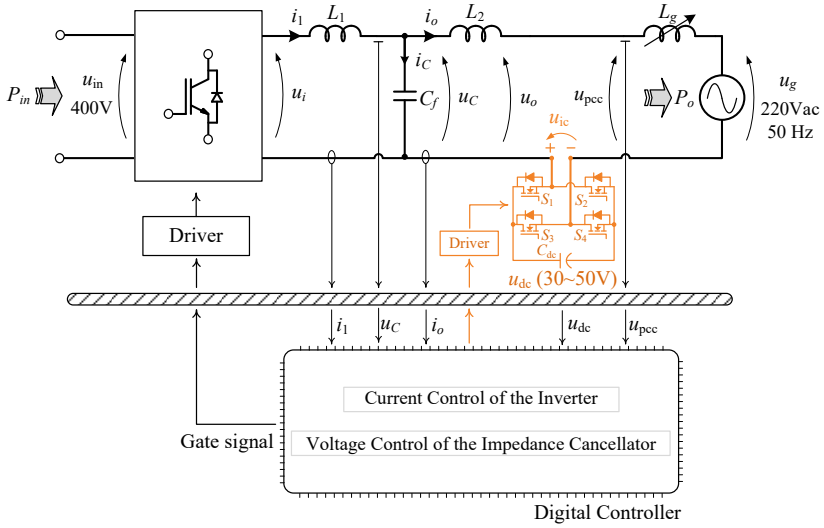

Fig. 2 Proposed inverter system configuration with the grid impedance cancellator.

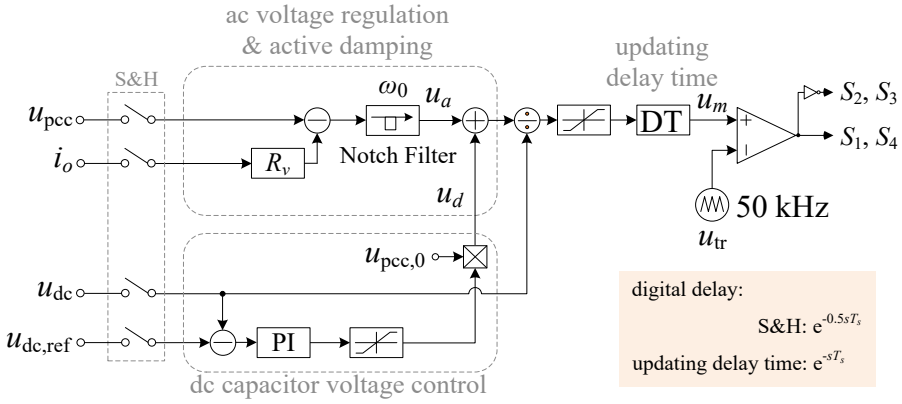

Fig. 3 Control block diagram of the grid impedance cancellator.

To suppress the effect of the filter resonance on the inverter performance, active damping function is also integrated into the impedance cancellator so as to ease the burden of the inverter control. The implementation of active damping function can be realized through simple proportional harmonic injected current feedback as shown in Fig. 3, where R_v represents the gain of the active damping function or the virtual resistance.

The expected value of virtual resistance R_v can be designed as

$$R_v = \frac{\omega_{r\_up}\ L_2 + \omega_{r\_down}\ (L_1 + L_2)}{2} \tag{1}$$

where $\omega_{r\_down} = \sqrt{\frac{1}{L_2\ C_f}}$ and $\omega_{r\_up} = \sqrt{\frac{L_1 + L_2}{L_1\ L_2\ C_f}}$.

Detailed derivation of (1) is given in the Appendix.

C. Modeling Analysis

By combining the ac voltage regulation and the active damping function as shown in Fig. 3, the corresponding generated output information, u_a, will be

$$\Delta U_a(s) = G_{NF}(s)\ e^{-0.5sT_S}\ \{\Delta U_{pcc}(s) - R_v\ [\Delta I_o(s) - \Delta I_{ref}(s)]\} \tag{2}$$

where $e^{-0.5sT_S}$ is the transfer function of the sampling-and-holding unit, and $G_{NF}(s)$ represents the notch filter written as

$$G_{NF}(s) = \frac{s^2 + \omega_0^{\ 2}}{s^2 + 2\omega_b s + \omega_0^{\ 2}} \tag{3}$$

in which the center line frequency ω_0 is generated from the phase locked loop (PLL) in the inverter controller and the band ω_b determines the response time of the filter. The generated output signal based on the dc capacitor voltage feedback loop is calculated as

$$\Delta U_d(s) = \Delta U_{g,0}(s)\ G_{PI}(s)\ e^{-0.5sT_S}\ [\Delta U_{dc}(s) - \Delta U_{dc,ref}(s)] \tag{4}$$

where $G_{PI}(s)$ is the transfer function of proportional-integral (PI) controller and the sinusoidal signal, $\Delta U_{g,0}$, is used to force the dominant line frequency component at the ΔU_d. Thus, the cut-off frequency of PI controller should be designed to be much lower than the line frequency.

By integrating (2) and (4), the modulating signal, ΔU_m, is derived as

$$\Delta U_m(s) = \frac{[\Delta U_a(s) + \Delta U_d(s)]}{\Delta U_{dc}\ e^{-0.5sT_S}} e^{-sT_S} = \frac{[\Delta U_a(s) + \Delta U_d(s)]}{\Delta U_{dc}} e^{-0.5sT_S} \tag{5}$$

Thus, the converter output voltage of the impedance cancellator is

$$\Delta U_{ic}(s) = [\Delta U_a(s) + \Delta U_d(s)]\ e^{-0.5sT_S} \tag{6}$$

Considering that the control bandwidth of the dc capacitor voltage feedback loop is designed to be much lower because the line frequency, ΔU_d can be neglected and eq. (6) is simplified into

$$\begin{aligned} \Delta U_{ic}(s)\big|_{\Delta U_d(s)\cong 0} &= \Delta U_a(s)\ e^{-0.5sT_S} \\ &= G_{NF}(s)\ e^{-sT_S}\ \{\Delta U_{pcc}(s) - R_v\ [\Delta I_o(s) - \Delta I_{ref}(s)]\} \\ &\cong G_{NF}(s)\ e^{-sT_S}\ [\Delta U_{pcc}(s) - R_v\ \Delta I_o(s)] \\ &= e^{-sT_S}\ [\Delta U_{pcc,h}(s) - R_v\ \Delta I_{o,h}(s)] \end{aligned} \tag{7}$$

Based on (7), the equivalent circuit is obtained by separating the ac voltage regulation (or the equivalent grid impedance cancellation) and the active damping function as

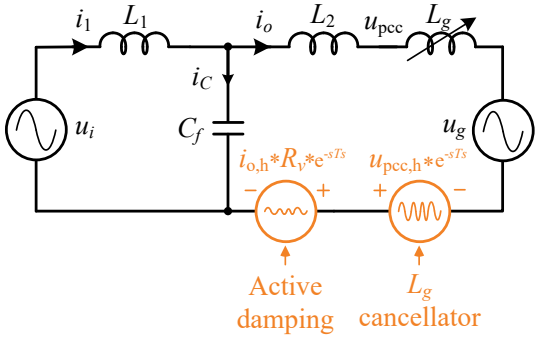

(a) Equivalent voltage source.

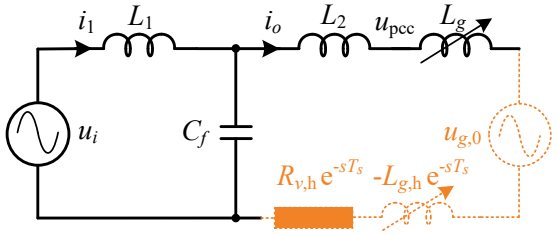

(b) Equivalent impedance.

Fig. 4 Equivalent circuit of the grid impedance cancellator.

presented in Fig. 4(a). Then, the corresponding physical meaning can be represented by the equivalent impedance as shown in Fig. 4(b), in which $u_{g,0}$ represents the line frequency component of the grid voltage, the virtual resistance, $R_{v,h} = R_v\ e^{-sT_S}$, is brought in by the active damping function, and the negative grid impedance, $L_{g,h} = L_g\ e^{-sT_S}$, is formed by the unity gain-based PCC harmonic voltage feedforward.

As shown in Fig. 4, both of the virtual resistance and the negative grid impedance are relevant with the digital delay term, e^{-sT_S}. To examine the effect of the digital delay on them, the mathematical model of the original LCL filter and the reshaped one in regard of the grid impedance can be derived and evaluated comparatively. Following Fig. 1(b), the open-loop transfer function of the original LCL filter in regard of the grid impedance is derived as

$$G_{o,o}(s)=\frac{\Delta I_o(s)}{\Delta U_i(s)} =\frac{Z_C(s)}{Z_1(s)[Z_2(s)+Z_g(s)]+Z_1(s)Z_C(s)+[Z_2(s)+Z_g(s)]Z_C(s)} \quad (8)$$

After reshaping the impedance, the inserted series impedance by the grid impedance cancellator is

$$Z_{ic}(s)=G_{NF}(s)\,[R_v\ e^{-sT_S}+s\,L_g\ (1-e^{-sT_S})] \quad (9)$$

and thereby the open-loop transfer function of the reshaped "LCL filter" is expressed as

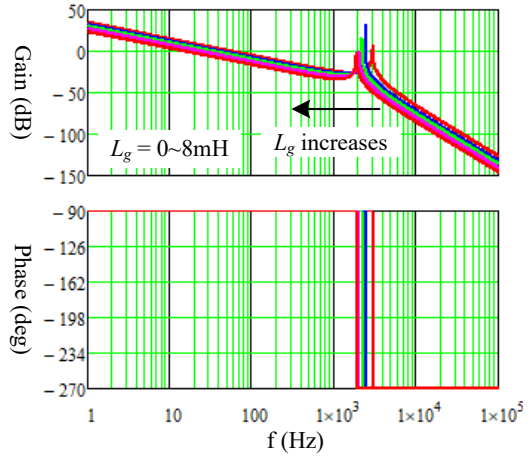

(a) Original LCL filter.

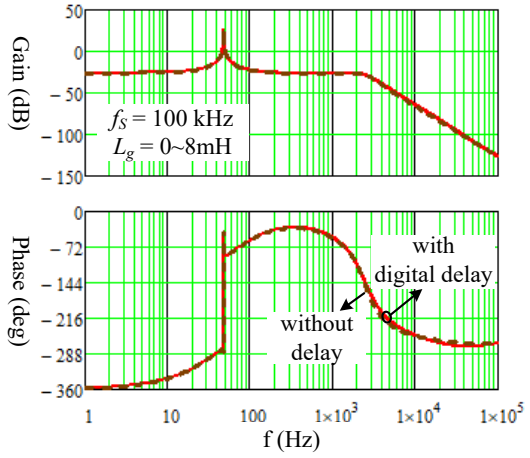

Reshaped "LCL filter".

Fig. 5 Open-loop transfer functions of the original LCL filter and the reshaped one with variable grid impedance.

$$G_{o,ic}(s)=\frac{\Delta I_o(s)}{\Delta U_i(s)} =\frac{Z_C(s)}{Z_1(s)[Z_2(s)+Z_{ic}(s)]+Z_1(s)Z_C(s)+[Z_2(s)+Z_{ic}(s)]Z_C(s)} \quad (10)$$

By replacing the filter parameters with the value tabulated in Table I, Eq. (8) and Eq. (10) are plotted as shown in Fig. 5, in which a set of frequency response of the reshaped "LCL filter" with the grid impedance cancellation is overlaid with each other. It indicates that 1) without the grid impedance cancellation, the filter resonant frequency varies widely with the variation of equivalent grid impedance, 2) with the grid impedance cancellation, the effect of equivalent grid impedance is eliminated, 3) with the active damping function, the filter resonance is well damped, and 4) the digital delay leads to minor impact on the impedance reshaping as presented in Fig. 5(b). Therefore, by neglecting the effect of minor digital delay, the reshaped grid-connected inverter with an LCL filter behaves as a well-damped one with the cancellation of equivalent grid impedance as revealed in Fig. 6.

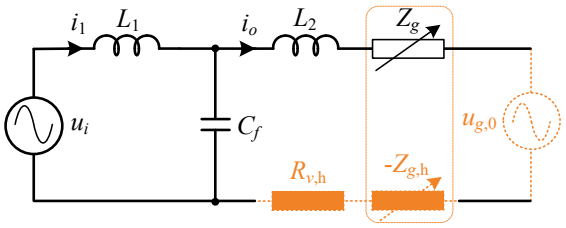

Fig. 6 Reshaped well-damped grid-connected inverter with the cancellation of Z_g.

III. Experimental Verification

A 125 V, 50 Hz inverter prototype with the proposed grid impedance cancellator has been built and evaluated for demonstration purpose. In the following tests, the grid-connected inverter is regulated using proportional-resonant-plus-harmonic-compensation (PR+HC)-based current control strategy with unity gain-based filter capacitor voltage feedforward.

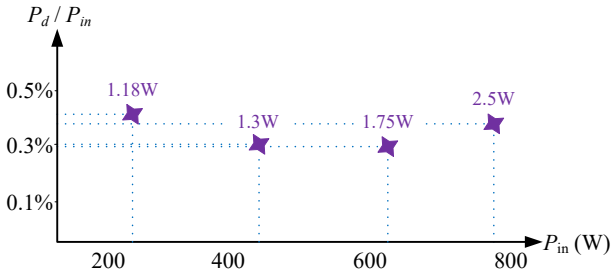

Fig. 7 Power loss of the cancellator as a function of the inverter input power.

Considering the extreme low dc capacitor voltage, switching devices of the impedance cancellator are selected as MOSFET FDD86110 (100V, 50A). Based on that, Fig. 7 shows the power consumption of the cancellator (P_d) measured by universal power analyzer, Voltech PM6000, as a function of the inverter input power (P_{in}), in which the power loss of the cancellator is mainly composed of switching devices and dc capacitors, and accounts for lower than 0.5% of the inverter input power. Thus, the efficiency of the entire system is not sacrificed owing to extreme low VA rating of the impedance cancellator.

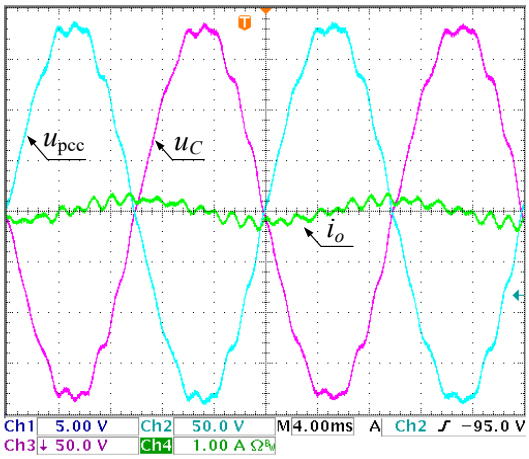

(a) Cancellator disabled.

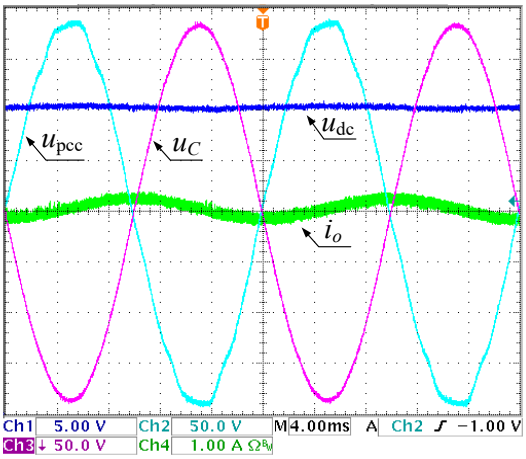

(b) Cancellator enabled.

Fig. 8 Key waveforms with the inverter disabled.

A. Key Waveforms with the Inverter Disabled

Figs. 8 presents the key waveforms when the grid-connected inverter is disabled. As seen in Fig. 8(a), due to the standby LC resonant tank at the grid side of the inverter, the oscillation appears at the grid current and the PCC voltage when the grid impedance cancellator is disabled. With the insertion of the grid impedance cancellator, the oscillation disappears as shown in Fig. 8(b) because of the inserted active

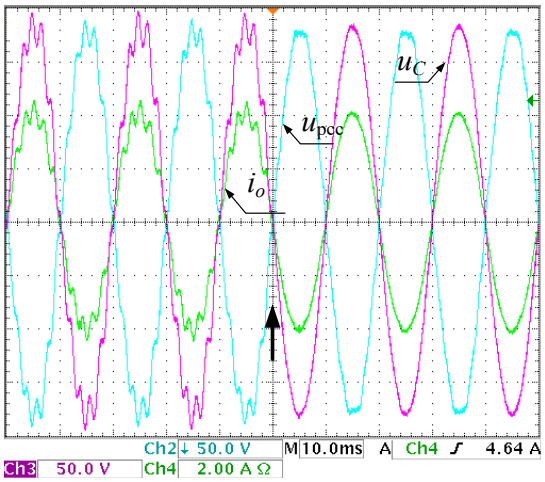

(a) Cancellator from disabled to enabled.

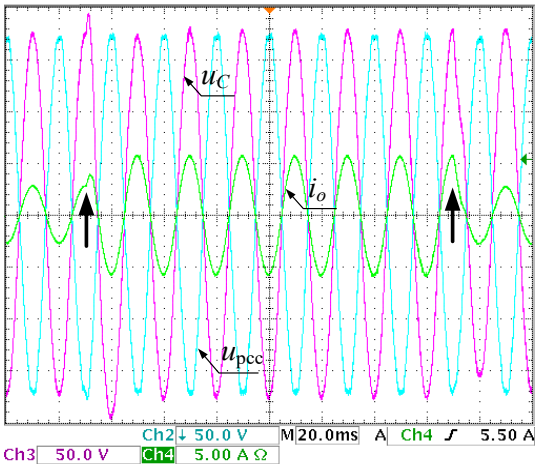

(b) Injected power transients.

Fig. 9 Dynamic behaviors of the grid-connected inverter when $L_g = 7.2$ mH .

damping function or virtual resistance as introduced in Sec. II. Moreover, it prevents the voltage at the inverter output from the harmonic one at the PCC successfully. Improvements of the inverter stability and harmonic rejection with the grid impedance cancellator will be validated in the following parts when the inverter is enabled.

B. Dynamic Behavior

Fig. 9(a) reveals that, when the impedance cancellator is disabled, the inverter is poor stable under the weak grid condition and the severe oscillation happens at both the PCC voltage and the injected current; when the cancellator is enabled, the oscillation disappears and the injected current becomes smooth because the grid impedance is cancelled and the harmonic voltage is suppressed at the filter capacitor voltage. Fig. 9(b) also indicates that the inverter operates well with the power transients even under the weak grid condition.

IV. CONCLUSIONS

The grid impedance cancellator consists of a full-bridge dc-ac converter without passive filtering elements is proposed. It has been proven to feature 1) full cancellation of equivalent grid impedance, 2) strong harmonic suppression against grid disturbance, and 3) active damping function to ease the burden of the inverter current control. Thus, the reshaped grid-connected inverter appears as a well-damped LCL filter without grid impedance. The experiment results show a good agreement with the theoretical analysis. In the future full paper, the theoretical modeling of the proposed system will be studied, and the power consumption of the grid impedance cancellator will be measured.

APPENDIX

Based on Fig. 6, the characteristic resonant frequency of the filter is changeable with different R_v. For example, in Fig. 6, if $R_v = 0\ \Omega$

$$\omega_{r\_up} = \sqrt{\frac{L_1 + L_2}{L_1\ L_2\ C_f}} \tag{A1}$$

where ω_{r_up} is the possible maximum characteristic resonant frequency, while if $R_v = \infty\ \Omega$, then

$$\omega_{r\_down} = \sqrt{\frac{1}{L_1\ C_f}} \tag{A2}$$

where ω_{r_down} is the possible minimum characteristic resonant frequency.

Secondly, the impedance of L_1 and $L_2 - R_v$ branch, $Z_{L(\mathrm{LCL})}$, is calculated as

$$Z_{L(\mathrm{LCL})}(s) = s\ L_1 \frac{s\ L_2 + R_v}{s\ (L_1 + L_2) + R_v} \tag{A3}$$

with the impedance feature as shown in Fig. 10.

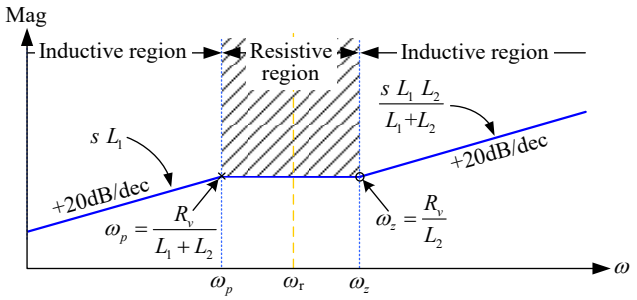

Fig. 10 Impedance feature of L_1 and $L_2 - R_v$ branch.

To find out the optimized quality factor (Q-factor), the range of changeable characteristic resonant frequency between (A1) and (A2) should fall into the shadow areas as shown in Fig. 10, which is the resistive region of L_1 and $L_2 - R_v$ branch [10]. Accordingly, based on (A3), the virtual resistance is limited with the range of

$$\frac{R_v}{L_1 + L_2} \le \omega_r \le \frac{R_v}{L_2} \tag{A4}$$

Supposing that the virtual resistance R_v changes from 0 Ω to ∞ Ω, it is deduced that,

$$\omega_{r\_down} \le \omega_r \le \omega_{r\_up} \tag{A5}$$

Combining (A4) and (A5), the selection criterion of the apparent virtual resistance is derived as

$$\begin{cases} \dfrac{R_v}{L_1 + L_2} \le \omega_{r\_down} \\ \dfrac{R_v}{L_2} \ge \omega_{r\_up} \end{cases} \tag{A6}$$

of which the optimized value of R_v is given as (1).

REFERENCES

[1] M. Liserre, F. Blaabjerg, and S. Hansen, "Design and control of an *LCL*-filter-based three-phase active rectifier," *IEEE Trans. Ind. Appl.*, vol. 41, no. 5, pp. 1281-1291, Sept./Oct. 2005.

[2] W. Wu, Y. He, and F. Blaabjerg, "An *LLCL* Power Filter for Single-Phase Grid-Tied Inverter," *IEEE Trans. Power Electron,* vol. 27, no. 2, pp. 782-789, Feb. 2012.

[3] D. Pan, X. Ruan, C. Bao, W. Li and X. Wang, "Capacitor-Current-Feedback Active Damping With Reduced Computation Delay for Improving Robustness of *LCL*-Type Grid-Connected Inverter," *IEEE Trans. Power Electron.*, vol. 29, no. 7, pp. 3414-3427, Jul. 2014.

[4] S.G. Parker, B.P. McGrath, and D.G. Holmes, "Regions of Active Damping Control for LCL Filters," *IEEE Trans. Ind. Appl.*, vol. 50, no. 1, pp. 424-432, Jan. /Feb. 2014.

[5] J.L. Agorreta, M. Borrega, J. Lopez, and L. Marroyo, "Modeling and Control of *N*-Paralleled Grid-Connected Inverters with LCL Filter Coupled Due to Grid Impedance in PV Plants," *IEEE Trans. Power Electron.*, vol. 26, no. 3, pp. 770-785, Mar. 2011.

[6] J. Enslin and P. Heskes, "Harmonic interaction between a large number of distributed power inverters and the distribution network," *IEEE Trans. Power Electron.*, vol. 19, no. 6, pp. 1586-1593, Nov. 2004.

[7] F. Wang, J.L. Duarte, M.A.M. Hendrix, and P.F. Ribeiro, "Modeling and Analysis of Grid Harmonic Distortion Impact of Aggregated DG Inverters," *IEEE Trans. Power Electron.*, vol. 26, no. 3, pp. 786-797, Mar. 2011.

[8] J. He, Y. Li, D. Bosnjak, and B. Harris, "Investigation and Active Damping of Multiple Resonances in a Parallel-Inverter-Based Microgrid," *IEEE Trans. Power Electron.*, vol. 28, no. 1, pp. 234-246, Jan. 2013.

[9] M. Lu, X. Wang, P.C. Loh, and F. Blaabjerg, "Resonance Interaction of Multiparallel Grid-Connected Inverters With LCL Filter," *IEEE Trans. Power Electron.*, vol. 32, no. 2, pp. 894-899, Feb. 2017.

[10] W. Wu, Y. He, T. Tang, and F. Blaabjerg, "A New Design Method for the Passive Damped LCL- and LLCL-Filter Based Single-Phase Grid-Tied Inverter," *IEEE Trans. Ind. Electron,* vol. 60, no. 10, pp. 4339-4350, Oct. 2013.